Triggered functional dynamics of AsLOV2 by time-resolved electron paramagnetic resonance at high magnetic fields

Shiny Maity[1+], Brad D. Price[2+], C. Blake Wilson[2], Arnab Mukherjee[3], Matthieu Stark[4], David Parker[4], Maxwell Z. Wilson[5], Janet E. Lovett[6], Songi Han[1*], and Mark S. Sherwin[2*]

[1]*Department of Chemistry and Biochemistry, UC Santa Barbara, Santa Barbara, CA 93106*
[2]*Department of Physics, UC Santa Barbara, Santa Barbara, CA 93106*
[3]*Department of Biological Engineering, UC Santa Barbara, Santa Barbara, CA 93106*
[4]*Department of Chemistry, University of Durham, Durham DH1 3LE, UK*
[5]*Department of Molecular, Cellular, and Developmental Biology, UC Santa Barbara, Santa Barbara, CA 93106*
[6]*School of Physics and Astronomy, University of St. Andrews, St. Andrews KY16 9SS, UK*

[+] denotes co-first author
[*] denotes corresponding authors
Songi Han songihan@ucsb.edu
Mark S. Sherwin sherwin@ucsb.edu.

Abstract

We present time-resolved Gd-Gd electron paramagnetic resonance (TiGGER) at 240 GHz for tracking inter-residue distance during a protein's mechanical cycle in solution state using Gd-sTPATCN spin labels. Gd-sTPATCN has a variety of favorable qualities that include a spin-7/2 EPR-active electron, a short linker, a narrow intrinsic linewidth, and virtually no anisotropy at high magnetic fields (8.6 T) when compared to nitroxide spin labels. Using TiGGER, we were able to determine that upon light activation, the Jα-helix and N-terminal of AsLOV2 separate in less than 1 s and relax back to equilibrium in approximately 60 s. We observed decoupling of the light activated photocycle from the long-range mechanical motions in Q513A-mutated AsLOV2 by comparing TiGGER data to time-resolved UV-Vis spectra. Our results suggest that TiGGER has the potential to become a valuable tool for the study of triggered functional dynamics in proteins that is complementary to existing methods.

1 Introduction

Proteins are fundamental building blocks of life. Understanding their function is key to understanding biological processes; this drive for understanding has resulted in nearly 190000 protein structures being logged into the Protein Data Base at the time of writing [1]. Most state-of-the-art structural biology tools require the protein to be immobilized (rapid freeze quench EPR, cryo-electron microscopy, etc.) or mechanically inhibited (X-ray crystallography) which may cause a significant amount of information to be lost (e.g. time-dependence, environmental effects, and pH effects) [2]. The thoroughness with which static structures have been mapped leads one to begin considering a functional "movie" – observing a number of biologically relevant amino acid sites move in real time – which can be combined to create a 3D rendition of site-specific motion. A satisfactory and complete movie, for the purpose of better understanding protein function and motion, requires real-time, *in vitro* tracking.

Time-resolved IR spectroscopy is able to provide information about the temporally-varying vibrational modes of constituent molecules, but lacks the ability to provide inter-residue distance information [3, 4]. In contrast, Förster resonance energy transfer (FRET) tracks distance-mediated fluorescence and has been widely used as a "spectroscopic ruler" to probe conformational dynamics of macromolecules by measuring nanoscale distances between two selective sites [5]. Though the physical mechanism elucidating distance is different, distance is "filmed" in a similar way to the techniques presented in this paper. Solution state NMR is another well-established method for studying distances in proteins at physiological conditions, but the smaller magnetic moment of the nuclear spin can only resolve distances up to 20-25 Å. High resolution NMR studies are often combined with lower resolution small angle X-ray (SAXS) and neutron scattering (SANS) measurements which can report on the overall dimension and shape of a biomolecule, and can therefore provide a combined holistic picture [6].

The biophysical method proposed in this paper complements these existing methodologies and yields qualitative, time-dependent mechanical motion through time-resolved Gd-Gd electron paramagnetic resonance (TiGGER) in a class of proteins known as the Light, Oxygen, and Voltage family (LOV), which undergoes reversible structural changes in response to stimulation. LOV proteins have

been used as optogenetic actuators to establish light-dependent control over various aspects of cellular function, but efficient actuator design requires an in-depth understanding of site-specific and inter-site movements *in vitro*, which cannot be adequately resolved with current biophysical techniques [7–10]. A comprehensive protein LOV movie would, for example, contain time-resolved secondary structure provided by trIR, high (Å)-definition movement provided by tr X-ray crystallography, and more natural, though lower definition, *in vitro* movement provided by FRET or high field Gd-Gd electron paramagnetic resonance (EPR) (as described here). We chose to focus specifically on a LOV protein from *Avena sativa* (AsLOV2) because of intense interest in the community at large about its potential as a genetically encoded molecular actuator [11–14]. Furthermore, AsLOV2 serves as an ideal test candidate for the transient continuous wave (cw) EPR technique presented here due to significant movement of the N-terminus away from the C-terminus upon light-activated Jα helix unfolding, and due to the relative simplicity to excite it using 450 nm illumination [7, 11, 12] (see Fig. 1, top).

Pioneering work of Steinhoff and Hubbell demonstrated that cwEPR may be used to track site-specific structural changes in proteins upon activation [15–17]. Such experiments made use of highly anisotropic nitroxide-based labels that provide extensive knowledge about the local environment that the spin label resides in. Label tumbling rate informs an experimentalist about the rigidity of the spin labeled residue in 3D space and mechanical activation of a protein may alter this rigidity. Figure 1 (bottom row) is an example of such an experiment, performed on AsLOV2 that is nitroxide labeled at surface site T406C or E537C: steady-state lineshape changes caused by a change in spin label tumbling rate (left) can be tracked as a function of time as a result of protein activation (right). These experiments are done in lifelike environments, but no information about changes in spin-spin distance separation is obtained, and hence no direct information about protein movement can be inferred. Double electron-electron resonance (DEER), on the other hand, uses nitroxides (and other labels) and can provide such distances, but requires cryogenic temperatures and thus eliminates many of the environmental effects on function [18].

Gd-sTPATCN is a high-spin ($S = \frac{7}{2}$), isotropic spin label with a short tether [19] that enables the observation of cryogenic and room temperature *in vitro* dipolar broadening due to its unique properties (see Figs. 2 and 3, bottom left) [20]. The linewidth of singly-Gd-labeled (SL) AsLOV2 is approximately 4 G (11 MHz), while dipolar broadening is $\omega_{dd}(r_{AB} = 3\text{ nm}) = 2\pi * 1.1$ MHz at a spin-spin distance of 3 nm, and therefore observable broadening is expected at this distance. Further, as shown in Clayton *et al.*, the high spin of Gd(III) increases dipolar sensitivity by increasing the energy of coupling (see Eqn. 2) and therefore increases the distance sensitivity accessible by TiGGER.

Specifically, the central transition of Gd(III), which dominates the cwEPR spectrum at high field, is narrowed with increasing B_0 and thereby shows increased dipolar sensitivity with increasing B_0. To first order in perturbation theory, $E^{(1)}_{ZFS}(-\frac{1}{2} \rightarrow \frac{1}{2}) = 0$, which means that the second order term $E^{(2)}_{ZFS}(-\frac{1}{2} \rightarrow \frac{1}{2}) = \frac{D^2}{g\mu_B B_0}$ becomes the leading order contribution to linewidth, and hence is inversely proportional to B_0 [19, 21]. The favorable high-spin and narrow linewidth properties of Gd labels have been extensively utilized for cryogenic-temperature DEER measurements [22–28]. This study extends the application of these characteristics to achieve *in vitro* real-time transient dipolar EPR spectroscopy.

We present TiGGER as a method for tracking spin-spin distance-mediated dipolar coupling. A change of spin environment, be it tumbling rate or local interactions, can be observed by change in the cwEPR lineshape. In order to observe a change in dipolar broadening, other line-broadening contributions must be sufficiently narrow and spin-spin dipolar coupling must be large [31], as provided by Gd-sTPATCN. We were able to make use of TiGGER to extract the room-temperature mechanical relaxation time of AsLOV2's C-terminus relative to its N-terminus after light-activation. These types of measurements are novel and are inaccessible using the more widely used nitroxide spin labels.

We selected residues 406 (N-terminus) and 537 (C-terminus) for initial studies by side-directed mutagenesis and spin labeling (SDSL) followed by transient cwEPR [1, 12]. Numerical simulations on Multiscale Modeling of Macromolecules (MMM) software (version 2018.2) show that when crystallized, nitroxide-based MTSL labels attached to residues 406 and 537 are $\sim$ 2.63 nm apart; it is unknown for certain how this changes in the solution state, but we expect it to remain similar ($\pm$0.4 nm) [32, 33]. In solution state, after light activation, the Jα-helix unfolds and it is expected that sites 406 and 537 become separated beyond the dipolar sensitivity of Gd-Gd cwEPR (approx. 4 nm) [11, 12, 34].

Assuming contributions from the zero-field splitting (ZFS) are negligible, a simple Hamiltonian that governs our spin system is given by

$$\mathcal{H} = \mathcal{H}_Z + \mathcal{H}_{dd} = \sum_{i=A,B} \omega_{ei} S_{zi} + \bar{S}_A \cdot \bar{\bar{T}} \cdot \bar{S}_B \qquad (1)$$

where the first term is the Zeeman term and the second term is the dipolar interaction between pairs of spins. The high field field approximation allows us to express the second term as

$$\mathcal{H}_{dd} = \omega^0_{dd} \left(S^A_z S^B_z - \frac{1}{4} \left(S^A_+ S^B_- + S^A_- S^B_+ \right) \right) \cdot \left(3\cos^2\theta_d - 1 \right) \qquad (2)$$

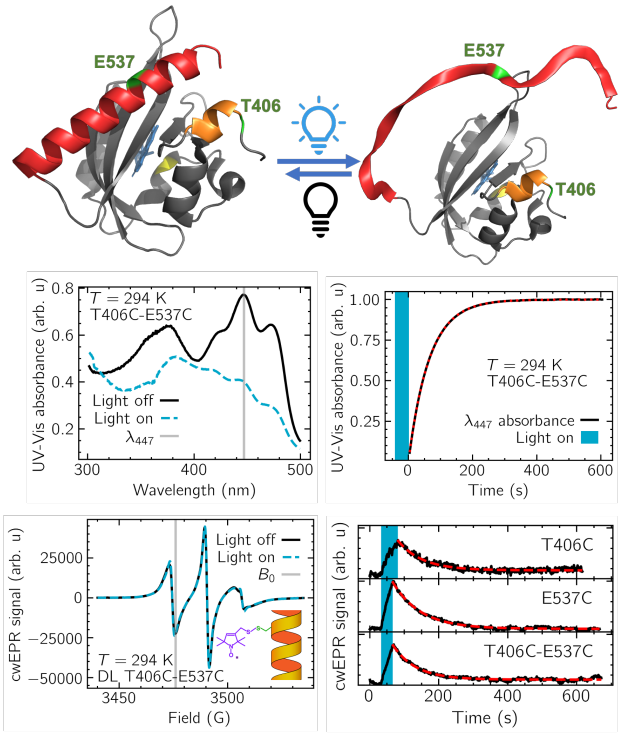

Figure 1: Photoresponse of AsLOV2. (top row) PYMOL-generated [29] (version 2.x; PDB 2V1A [30]) structure demonstrating AsLOV2 structural change (dark-state AsLOV2 shown left, lit-state AsLOV2 shown right) that occurs after 450 nm illumination. The lit state residues 537 and 406 are marked green on red Jα-helix (C-terminal) and orange N-terminal, respectively. (middle left) UV-Vis absorption spectra of AsLOV2 T406C-E537C with (dashed blue line) and without (solid black line) blue light activation (Thorlabs, Inc. LIU470A). The gray line indicates the wavelength at which the lifetime of the protein was measured. (middle right) The lifetime of the protein ($\tau = 65.06 \pm 0.03$ s) after activation with blue light was measured by recording the UV-Vis absorbance at 447 nm. (bottom left) cwEPR spectra of MTSL (a nitroxide-based standard EPR spin label) labeled AsLOV2 at the residues 537 and 406 at X-band. (bottom right) Transient X-band EPR demonstrating lack of effect of doubly versus singly MTSL-labeled AsLOV2. Time constants for the fits (dashed red lines) were $\tau_{T406C} = 70.1 \pm 1.3$ s, $\tau_{E537C} = 80.5 \pm 0.6$ s, $\tau_{T406C-E537C} = 66.2 \pm 0.8$ s. Transient data (solid black lines) and their fits showed no significant change in amplitude after light activation (solid blue lines) between singly (SL) and doubly-labeled (DL) samples. Field values used for time-dependent measurements were 3475 G for T406C and 3476 G for E537C and T406C-E537C. Experiments were completed at 294 K.

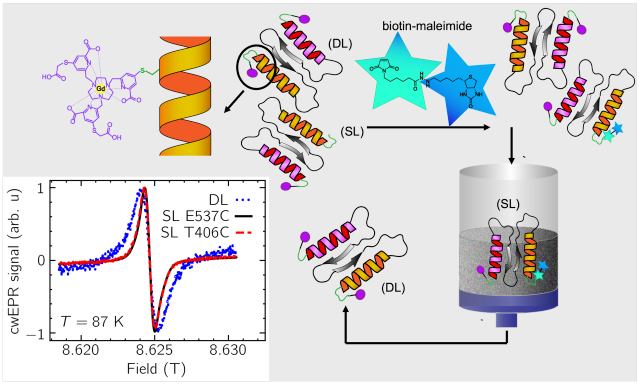

Figure 2: Site-directed spin labeling of AsLOV2 with Gd-sTPATCN. (in gray) Enrichment of the doubly-labeled AsLOV2 (DL T406C-E537C). The reaction products from the spin-labeling of DL T406C-E537C is mixed with biotin-maleimide and streptavidin-agarose. Non-fully labeled AsLOV2 with free cysteine gets trapped in the column with streptavidin-agarose and the fully labeled DL T406C-E537C gets through the column. (bottom left) Comparison of 240 GHz cwEPR lineshapes of AsLOV2 singly (SL) and doubly-labeled with Gd-sTPATCN. Lineshapes are normalized to individual maxima in order to highlight dipolar broadening of DL sample. Experiment was done at cryogenic temperatures to eliminate effects of motional averaging. Solid black line, dashed red line, dotted blue line correspond to AsLOV2 samples singly labeled at residue 537, singly labeled at residue 406, and DL at residue 537-406, respectively.

where $\omega^0_{dd} = \frac{\mu_0}{4\pi}\frac{\mu_b^2 g_1 g_2}{\hbar}\frac{1}{r^3_{AB}}$ is the dipolar splitting caused by one spin on another and θ_d is angle between $\vec{r_{AB}}$ and the applied field B_0 [21, 34]. $\mathcal{H}_{dd}$ expresses the fields felt by one spin, S_A, due to another, S_B, where a random distribution of S_B magnetic moments within the sample causes a small shift to the applied field ($B_{\text{eff},A} = B_0 + B_{dd}$) and therefore an inhomogeneous broadening of the cwEPR resonance spectrum. Increasing the ensemble-averaged spin-spin separation, r_{AB}, reduces the dipolar contribution to the spectrum and thereby narrows the cwEPR line. The distance dependence of the dipolar coupling is commonly applied in DEER to measure static inter-spin distance, but may be extended to cwEPR for real-time tracking of ensemble-averaged spin-spin separation, assuming, for example, that $\mathcal{H}_{\text{ZFS}}$, $\mathcal{H}_{\text{hyperfine}}$, ... $\ll \mathcal{H}_{dd}$. An important note about equation (2) is that it will average to zero with fast tumbling [35]. Hence, the condition $\omega_{dd} * \tau > 1$, where τ is the rotational correlation time, is a requirement for observing dipolar broadening that is not averaged out in solution state by cwEPR.

2 Results

Following site-directed mutagenesis, the two sites, 406 and 537, were mutated to cysteine residues and spin-labeling procedure was carried out to label these sites (T406C and E537C) with nitroxide spin label (MTSL) (1-Oxyl-2,2,5,5-tetramethyl-Δ3-pyrroline-3-methyl methanesulfonothioate) or Gd-sTPATCN.

To remove any AsLOV2 protein that was not fully labeled in the above steps, a method to enrich the amount of doubly-labeled (DL) protein was devised (Fig. 2, gray). For this purpose, spin-labeled preparation was further incubated with 0.01 mg/mL maleimide-biotin stock solution (prepared in 20 mM Tris-HCl 150 mM NaCl pH: 8.00) to achieve a 1:1 molar ratio between AsLOV2 cysteines and the maleimide-biotin. The mixture was incubated at room temperature for 50 min to allow the maleimide-biotin to react with any free (*i.e.*, unlabeled) cysteines in AsLOV2. Excess biotin-maleimide is not used in this step, so that biotin-maleimide has limited interaction with the photoactive cysteine. After incubation, the mixture was added to a streptavidin agarose resin (Pierce®, Thermo Scientific) to bind with biotinylated AsLOV2, thereby allowing DL AsLOV2 proteins to be enriched in the flow-through. (Fig. 2, gray). See demonstration of additional dipolar broadening in DL-Gd-sTPATCN-AsLOV2 as a result of enrichment in S.I. Fig. 1. The large DEER modulation depth (∼0.4) observed at Q-band (34 GHz Bruker E580 ELEXSYS pulse EPR spectrometer equipped with a TWT amplifier at 300 W) of the doubly-MTSL-labeled AsLOV2 indicated that we had sufficiently high labeling efficiency (conservatively ∼ 80% of the protein are double-labeled, as calculated from [36]) (see SI Fig. 4).

High-field EPR was carried out at UCSB's Institute for Terahertz Science and Technology (ITST). ITST's home-built EPR spectrometer consists of a 12.5 T field-swept magnet (Oxford Instruments), 60 mW 240 GHz cw source, and subharmonically mixed heterodyne receiver (Virginia Diodes, Inc., Charlottesville, VA) that operates in induction mode and has been described in detail previously [20, 37]. A small offset of the recorded magnet field of approximately 12 mT causes resonances shown in Figs. 2, 3 to appear at 8.62 T, not 8.608 T as would be expected for Gd labels with an isotropic g-value of 1.992 [38]. A 240 GHz Gaussian beam was coupled by a corrugated waveguide into the sample space, where liquid samples were loaded into a 100 μm-thick, 2-by-6 mm borosilicate glass capillary (VitroCom, Mountain Lakes, NJ) to maximize the ratio of optical surface area to optical density [39]. Capillaries were then placed on a Teflon® tape-covered, 7 mm wide, protected silver mirror. Field-swept EPR experiments were done at first in the dark and then under 450 nm laser illumination. The laser produced 70 mW at 450 nm (Laser Components USA, Inc., Bedford, NH) and was coupled into a fiber optic that carried approximately 15 mW to the sample space. Time-dependent experiments were completed by continuously collecting field-modulated, lock-in detected, cwEPR data as a function of time (60 ms time steps) and activating the laser light for 10 cycles of 5 seconds on, 175 seconds off. The repetitions were then averaged to reduce noise fluctuations (see SI section 2.1).

Using TiGGER, were able to observe EPR-detected intra-molecular light activated mechanical movement in AsLOV2 with time-dependent dipolar broadening of Gd(III). Figure 3 (bottom left) demonstrates the effect of dipolar broadening by spin labels placed at sites T406C and E537C located in the N and C termini respectively (see Fig. 1, top) [1]. As compared to singly labeled proteins (Fig. 3, top row), where no light-activated change was observed, the DL sample had significant field-swept lineshape change. In Figure 3 (bottom right) transients, using TiGGER, the time-dependent changes caused by light activation were elucidated. We observed a large time dependent light activation ($\tau_{\text{activate}} < 1$ s) and relaxation in the dark ($\tau_{\text{relax}} = 51.9 \pm 0.3$ s) in the DL sample, and little to no change in either SL or C450A-modified DL samples (discussed below). The sensitivity to specifically DL AsLOV2 means that we are explicitly measuring distance-mediated dipolar coupling and not a change in tumbling rate or sample temperature, for example.

To further confirm that we were explicitly measuring a change in solution state mechanical distance, we completed UV-Vis, X-band, and cryogenic temperature cwEPR measurements as comparisons. First, we expected that UV-Vis decay lifetimes would be comparable to that of the mechanical relaxation and used UV-Vis to confirm that the protein was indeed photoswitching. UV-Vis data is shown in Figure 1 (middle row): wavelength swept data of spin-labeled proteins showed results similar to that in the literature [7, 40] and a decay constant ($\tau = 65.06 \pm 0.03$ s) similar to what was observed with TiGGER. Next, X-band EPR (Fig. 1, bottom row) also gave similar time-dependent results (top: $\tau_{T406C} = 70.1 \pm 1.3$ s, middle: $\tau_{E537C} = 80.5 \pm 0.6$ s, bottom: $\tau_{T406C-E537C} = 66.2 \pm 0.8$ s) to that of TiGGER. However, the peak intensities of the lineshape changes were unchanged between single and double labeling, which means that the decay we observed was a result of changing tumbling rate when the J-α and A-α helices unfold, and not dipolar coupling. We confirmed that TiGGER is measuring mechanical movement, and that it is dipolar-mediated, proven by the large change between single and DL samples. Finally, cryogenic temperature measurements comparing singly and doubly-Gd-labeled samples were completed to confirm that dipolar broadening is apparent when rotational averaging has been eliminated. The results, shown in Figure 2 (bottom left) demonstrate a broadening of singly labeled 7 G linewidth to DL 12 G

and ensure that samples had multiple Gd-sTPATCN labels within TiGGER's distance sensitivity.

Further, similar high-field TiGGER experiments were completed on DL AsLOV2 with an additional C450A mutation. Previous studies have shown that mutation of this conserved cysteine residue leads to complete inhibition of the photocycle and suppression of the associated secondary structural changes [10, 41]. Our hfEPR experiments on C450A DL AsLOV2 shows no field-swept or time-dependent line shape changes and endorses these results (Fig. 3, bottom right and S.I. Fig. 8).

We also completed similar experiments of time-dependent hfEPR on Q513A-mutated DL AsLOV2. This glutamine residue (Q513) is located on the Iβ-sheet that interacts with the Jα-helix and is also in the immediate proximity of the chromophore binding site. It is suspected that, upon light activation, this glutamine residue switches its hydrogen bonding pattern with the chromophore and plays a key role in transmission of stress to the Jα-helix, which causes it to unfold [42, 43]. In order to elucidate the role of Q513 in the unfolding of the Jα-helix, we mutated the glutamine residue to an uncharged, non-polar amino acid, alanine, and observed site-specific intra-molecular mechanical movement in AsLOV2, across the same Gd (III) sites T406C and E537C as used before. The Q513A mutation slowed the kinetics of the chromophore photocycle by a factor of 5.97 ($\tau_{\text{Q513A DL}} = 388.4 \pm 0.5$ s) compared to the DL AsLOV2 ($\tau_{\text{DL}} = 65.0 \pm 0.3$ s) but did not inhibit photoswitching (see Fig. 4, right). In fact, the amplitude of change in UV-Vis absorption is similar between the wild type (referred to as DL for double labeling across T406C-E537C) and the Q513A variant (referred to as Q513A DL). This result is in agreement with previous UV-Vis photocycle kinetic studies on AsLOV2 Q513A [12]. However, Q513A mutation completely eliminated all hfEPR dipolar broadening effects and no field-swept nor time-dependent lineshape changes could be observed. This reinforces the earlier studies on AsLOV2 using time-resolved vibrational spectroscopy, where the frequency at 1640 cm^{-1} corresponding to the α-helix amide-I vibration mode is suppressed on light activation, compared to the wild-type protein [41, 44]. Our results directly show that the Q513 residue plays a critical role in modulating the structural changes of Jα-helix upon blue light illumination.

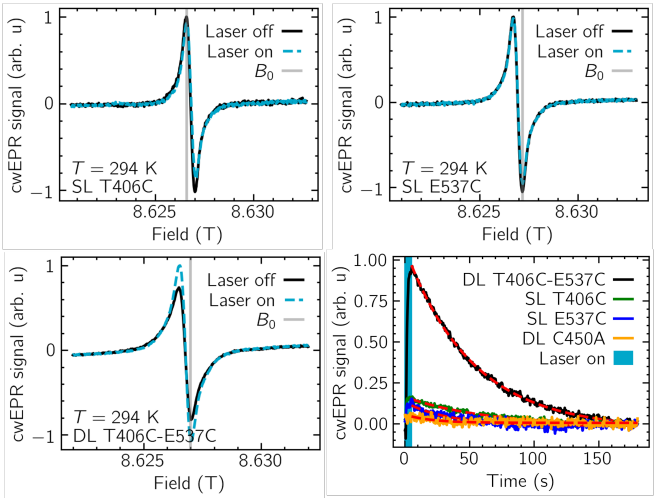

Figure 3: Effect of laser illumination on cwEPR spectra of Gd-labeled AsLOV2. Singly labeled (SL) cwEPR of residue 406 (top left), residue 537 (top right) spectra of AsLOV2 demonstrating that the spectrum with the laser off (solid black line) is unchanged when the laser is turned on (dashed blue line). (bottom left) DL (sites 406 and 537) cwEPR spectra of AsLOV2 demonstrating that the spectrum with the laser off (solid black line) is narrowed when the laser is turned on (dashed blue line). Static field B_0 where maximum time-dependent change occurred is shown on all three plots by vertical gray line. Note that the field values for for time-dependent measurements were not the same for all three samples. Though both derivative peaks (absorption shoulders) showed very similar time-dependent changes, the position with best signal-to-noise was chosen for the time-dependent figure; these were the low-field peak for T406C and the high-field peak for E537C and T406C-E537C. (bottom right) cwEPR time-dependent signal change of singly labeled and doubly-Gd-labeled AsLOV2 due to laser illumination at $T = 294$ K, shown by solid blue line (solid black, green, and blue lines correspond to singly labeled T406C, singly labeled E537C, and DL T406C-E537C, respectively). Overlaid best fits (dashed red lines) of the exponentials provide time constants of $\tau = 62.5 \pm 1.8$ s for SL T406C, $\tau = 34.6 \pm 1.9$ s for SL E537C, $\tau = 51.9 \pm 0.3$ s for DL T406C-E537C, and $\tau = 20.8 \pm 3.4$ s for DL C450A T406C-E537C, where the range represents a 95% confidence interval for the best fit. All plots are normalized to magnitude of DL T406C-E537C signal change. Static field for time-dependent experiments are shown in cwEPR field swept spectra with vertical gray line.

3 Discussion

This paper reports the ability of time-resolved Gd-Gd electron paramagnetic resonance to track mechanical separation of two protein residues upon activation. We were able to resolve an approximate time of activation and a precise relaxation time (that is consistent with UV-Vis relaxation) in AsLOV2 during and after 450 nm illumination. Gd-sTPATCN enhanced distance sensitivity as compared

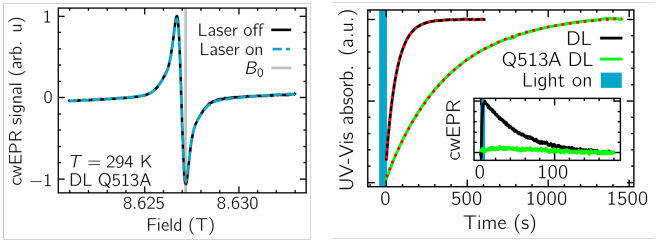

Figure 4: Q513A decoupling of chromophore and mechanical photocycles as detected by TiGGER. (left) cwEPR spectra of DL T406C-E537C-Q513A AsLOV2 showing no change between dark state (solid black line) and illuminated (dashed blue line). (right) Time-resolved UV-Vis demonstrates a slowing of the chromophore photocycle in unlabeled T406C-E537C after illumination (shown by vertical blue line). Solid black and solid blue represent DL T406C-E537C and Q513A DL T406C-E537C, respectively. Best fits are shown by dashed red lines with respective time constants of $\tau_{\text{DL}} = 65.0 \pm 0.3$ s and $\tau_{\text{Q513A DL}} = 388.4 \pm 0.5$ s. Static field for time-dependent experiment is shown left with vertical gray line. (inset) AsLOV2 time-dependent cwEPR signal change caused by laser illumination of AsLOV2 with and without Q513A mutation demonstrating that Q513A stabilizes C-terminus covalent adduct and inhibits mechanical motion. UV-Vis and EPR experiments were done at 294 K.

to EPR standard labels and allowed us to extract dipolar broadening at temperatures that are otherwise inaccessible. TiGGER allows researchers to probe the steps of a protein's photocycle in a lifelike environment, both at room temperature and in solution state and helps complete a picture that is partially told by X-ray crystallography, time-resolved IR spectroscopy, cryo-EM, time-resolved NMR, rapid freeze-quench EPR, and FRET.

Upon light activation, the FMN (flavin mononucleotide) chromophore is excited to a triplet state and reacts with the nearby C450 residue. It forms a covalent bond between the C(4a) atom of the chromophore and the sulfur atom of C450 [45]. This cysteinyl adduct formation is accompanied by destabilization of the Jα-helix in the C-terminal of the protein. We successfully probed the light activated movement of Jα-helix from the N terminal in AsLOV2 as a function of time (ms to s timescales), taking advantage of the spin properties of Gd-sTPATCN at high field. Though small, compared to the DL T406-E537C sample, it is worth noting that we see nonzero temporal decay of the singly labeled samples, which was unexpected. It is hypothesized that these small lineshape changes can be attributed to a small percentage of spins experiencing unintended dipolar broadening and subsequent narrowing that may be a result of nonspecific labeling. If a small number of unintended sites were being labeled, it is possible that they could move away from the intentionally labeled site upon light activation.

We expect that the narrowing effect caused by the activation of DL proteins is greater than is shown in Figure 3, but is obscured by a large background caused by imperfect labeling and protein activation. Even after purification, it is likely that a large fraction of the proteins were still singly labeled and caused a large, sharp background to obscure the desired DL lineshape change. Further, it is known that not all proteins will activate upon illumination, as a small fraction have a labeled central cysteine (see later discussion of C450A mutation) and others are be empty (without FMN chromophone), both of which will inhibit protein movement and contribute only a broadened background that obscures the signal of interest. We are currently modifying and enabling CWdipfit [46] (dipolar distance extraction software backed by EasySpin [47]) to help us eliminate these effects and extract only the DL broadening component of our experimental results. Further, solution state, room temperature experiments fall victim to rotational averaging; we were able to see signal change with the current samples, but rotational immobilization in hydrogels may limit tumbling and enhance signal sensitivity without sacrificing the protein's range of mechanical motion. Our signal sensitivity is also expected to improve as we refine our sample preparation protocol.

In LOV domains, the recovery rates of the covalent adduct to the dark state vary widely, on a timescale of seconds to days [40, 48–50]. This widely varying photocycle is interesting; it is believed that the adduct decay is base-catalyzed, limited by a proton transfer step [51]. The presence of a glutamine residue, Q513, in hydrogen-bonding interaction with the chromophore seems to be the only residue in proximity to the chromophore, capable of catalyzing this deprotonation process [42]. Hence, it is expected that mutation of Q513 to a non-polar residue will eliminate the photocycle. However, our UV-Vis experiments on Q513A AsLOV2 (see Fig. 4, right), along with the previous studies by others [12, 43], show that mutation to the glutamine residue slows the photocycle instead of prohibiting it. Studies in the literature have suggested that this could be potentially explained by effects of hydration of the LOV domain, where water molecules can directly act as a base catalyst by entering the chromophore binding pocket and hydrogen-bonding with the FMN chromophore [40, 52–54]. Indeed, we observed that the photocycle is still able to proceed even in the absence of the glutamine residue, albeit with a greater time constant (see Fig. 4). However, we did not observe any lineshape changes in the time-dependent hfEPR experiments. We attribute this to inhibited mechanical motion and a decoupling of the chromophore and mechanical photocycle – a finding that may be interesting to the optogenetic community. This indicates that the spectroscopic changes due to water-based catalysis at the FMN molecule in Q513A is not sufficient

to drive long-range movements, suggesting that Q513 is involved in more than just catalysis, but also helps drive the mechanical movement between N and C termini. Therefore, our hfEPR experiments on Q513A DL AsLOV2 were capable of directly confirming that the glutamine residue acts as an essential link for coupling the FMN photocycle at the core of the protein to driving the mechanical motion further away in the Jα-helix [41, 44].

Here we report a hfEPR method using Gd-sTPATCN spin labels that is capable of tracking distance-mediated *in vitro* mechanical motion in a LOV protein. To our knowledge, such measurements are only possible in solution state with TiGGER and FRET. FRET relies on the distance-dependent non-radiative energy transfer from donor to acceptor fluorophores that have been introduced site-specifically into the macromolecule of interest. Recent advances have also made it possible for its application on a single molecule level [55, 56]. However, the application of FRET to explore dynamics in a light sensitive protein can be complicated due to the need for additional correction factors to resolve the spectral crosstalk between the light sensitive protein and donor-acceptor pairs [57]. As well, FRET has a steeper distance falloff (r^{-6} vs. r^{-3}) than the technique we present in this paper [5, 58].

Future work for TiGGER will include refining the labeling protocol to enhance signal strength, incorporating a hydrogel for rotational stabilization, testing a variety of residues to create a 3D "movie" of mechanical motion, and upgrading the spectrometer to enable 10 μs-resolution field-swept spectra. Currently, transient measurements have a temporal resolution of $\sim$ 60 ms and can only be done at a fixed field. Enabling rapidscan EPR with complete digitization of the field-swept line every 10 μs, combined with an improved version CWdipfit [46], will enable quantitative time-dependent distance extraction and enhance the data presented by a TiGGER "movie".

4 Conclusion

In this paper, we demonstrate the first step to 'filming' a protein in action using TiGGER. Site-specific labeling allowed us to track a change in distances between residues in an ensemble of room temperature proteins. Additionally, we discovered mutation-induced decoupling of chromophore and mechanical photocycles, highlighting the importance of TiGGER to the optogenetic community. Future work, including improving the temporal resolution of the spectrometer and acquiring full time-dependent field swept spectra, may allow for extraction of absolute spin-spin distances in real-time during a protein's photocycle. Further, a more comprehensive and quantitative understanding of the effects of motional averaging at room temperature in solution state would enable more accurate quantitative distances. Additional experimental development and an application of TiGGER to a range of protein residues will enable three-dimensional, time-dependent mapping of protein mechanical action and may play an important role in improving design of optogenetic actuators and fluorescent reporters. Additionally, the technique presented here should be applicable to protein conformational changes that are triggered by other factors, such as ligand binding by rapid mixing, voltage actuation, or temperature jump as they become of interest to the community.

5 Acknowledgements

The authors would like to gratefully acknowledge support from the NSF though grant SMNF7Z-8-444063-21358 and the UC Office of the President Multicampus Research Programs and Initiatives under MRI-19-601107 for the development of the trEPR technology and the core research presented here. Some biochemical studies of AsLOV2 were supported by the NIH MIRA through grant R35GM136411. Figures were created in Python using SciencePlots [59].

References

[1] Protein Data Bank.

[2] J. W. Taraska, *Current Opinion in Structural Biology*, Engineering and design / Membranes **2012**, *22*, 507–513.

[3] E. Ritter, L. Puskar, F. Bartl, E. Aziz, P. Hegemann, U. Schade, *Frontiers in Molecular Biosciences* **2015**, *2*.

[4] M. L. Groot, L. J. G. W. van Wilderen, M. Di Donato, *Photochemical & Photobiological Sciences* **2007**, *6*, 501.

[5] C. E. Rowland, C. W. Brown, I. L. Medintz, J. B. Delehanty, *Methods and Applications in Fluorescence* **2015**, *3*, 042006.

[6] O. Duss, M. Yulikov, F. H. T. Allain, G. Jeschke in *Methods in Enzymology*, (Eds.: S. A. Woodson, F. H. T. Allain), Structures of Large RNA Molecules and Their Complexes, Academic Press, **2015**, pp. 279–331.

[7] A. Pudasaini, K. K. El-Arab, B. D. Zoltowski, *Frontiers in Molecular Biosciences* **2015**, *2*.

[8] D. Strickland, X. Yao, G. Gawlak, M. K. Rosen, K. H. Gardner, T. R. Sosnick, *Nature Methods* **2010**, *7*, 623–626.

[9] A. Mukherjee, K. B. Weyant, J. Walker, C. M. Schroeder, *Journal of Biological Engineering* **2012**, *6*, 20.

[10] S. M. Harper, L. C. Neil, K. H. Gardner, *Science* **2003**, Publisher: American Association for the Advancement of Science, DOI 10.1126/science.1086810.

[11] J. N. Iuliano, J. T. Collado, A. A. Gil, P. T. Ravindran, A. Lukacs, S. Shin, H. A. Woroniecka, K. Adamczyk, J. M. Aramini, U. R. Edupuganti, C. R. Hall, G. M. Greetham, I. V. Sazanovich, I. P. Clark, T. Daryaee, J. E. Toettcher, J. B. French, K. H. Gardner, C. L. Simmerling, S. R. Meech, P. J. Tonge, *ACS Chemical Biology* **2020**, *15*, Publisher: American Chemical Society, 2752–2765.

[12] J. P. Zayner, C. Antoniou, T. R. Sosnick, *Journal of Molecular Biology* **2012**, *419*, 61–74.

[13] O. I. Lungu, R. A. Hallett, E. J. Choi, M. J. Aiken, K. M. Hahn, B. Kuhlman, *Chemistry & Biology* **2012**, *19*, 507–517.

[14] L. Geng, J. Shen, W. Wang, *Chemical Communications* **2021**, *57*, Publisher: Royal Society of Chemistry, 8051–8054.

[15] H.-J. Steinhoff, R. Mollaaghababa, C. Altenbach, K. Hideg, M. Krebs, H. G. Khorana, W. L. Hubbell, *Science* **1994**, *266*, Publisher: American Association for the Advancement of Science, 105–107.

[16] R. Mollaaghababa, H.-J. Steinhoff, W. L. Hubbell, H. G. Khorana, *Biochemistry* **2000**, *39*, 1120–1127.

[17] C. Altenbach, K. Cai, J. Klein-Seetharaman, H. G. Khorana, W. L. Hubbell, *Biochemistry* **2001**, *40*, Publisher: American Chemical Society, 15483–15492.

[18] G. Jeschke, *Annual Review of Physical Chemistry* **2012**, *63*, 419–446.

[19] A. Shah, A. Roux, M. Starck, J. A. Mosely, M. Stevens, D. G. Norman, R. I. Hunter, H. El Mkami, G. M. Smith, D. Parker, J. E. Lovett, *Inorganic Chemistry* **2019**, *58*, 3015–3025.

[20] D. T. Edwards, Z. Ma, T. J. Meade, D. Goldfarb, S. Han, M. S. Sherwin, *Physical Chemistry Chemical Physics* **2013**, *15*, 11313.

[21] A. Feintuch, G. Otting, D. Goldfarb in *Methods in Enzymology*, (Eds.: P. Z. Qin, K. Warncke), Electron Paramagnetic Resonance Investigations of Biological Systems by Using Spin Labels, Spin Probes, and Intrinsic Metal Ions, Part A, Academic Press, **2015**, pp. 415–457.

[22] Y. Yang, F. Yang, Y.-J. Gong, J.-L. Chen, D. Goldfarb, X.-C. Su, *Angewandte Chemie International Edition* **2017**, *56*, 2914–2918.

[23] E. H. Yardeni, T. Bahrenberg, R. A. Stein, S. Mishra, E. Zomot, B. Graham, K. L. Tuck, T. Huber, E. Bibi, H. S. Mchaourab, D. Goldfarb, *Scientific Reports* **2019**, *9*, 12528.

[24] D. Goldfarb, *Physical Chemistry Chemical Physics* **2014**, *16*, 9685.

[25] A. Doll, M. Qi, N. Wili, S. Pribitzer, A. Godt, G. Jeschke, *Journal of Magnetic Resonance* **2015**, *259*, 153–162.

[26] D. T. Edwards, T. Huber, S. Hussain, K. M. Stone, M. Kinnebrew, I. Kaminker, E. Matalon, M. S. Sherwin, D. Goldfarb, S. Han, *Structure* **2014**, *22*, 1677–1686.

[27] A. Dalaloyan, M. Qi, S. Ruthstein, S. Vega, A. Godt, A. Feintuch, D. Goldfarb, *Physical Chemistry Chemical Physics* **2015**, *17*, 18464–18476.

[28] T. Bahrenberg, Y. Yang, D. Goldfarb, A. Feintuch, *Magnetochemistry* **2019**, *5*, Number: 1 Publisher: Multidisciplinary Digital Publishing Institute, 20.

[29] PyMOL, https://pymol.org/2/.

[30] RCSB PDB - 2V1A: N- and C-terminal helices of oat LOV2 (404-546) are involved in light-induced signal transduction (room temperature (293K) dark structure of LOV2 (404-546)), en-US.

[31] D. Nohr, R. Rodriguez, S. Weber, E. Schleicher, *Frontiers in Molecular Biosciences* **2015**, *2*.

[32] G. Jeschke, MMM, https://epr.ethz.ch/software.html.

[33] G. Jeschke, *Protein Science* **2018**, *27*, 76–85.

[34] J. A. Clayton, M. Qi, A. Godt, D. Goldfarb, S. Han, M. S. Sherwin, *Physical Chemistry Chemical Physics* **2017**, *19*, 5127–5136.

[35] M. H. Levitt, *Spin dynamics: basics of nuclear magnetic resonance*, 2nd ed., John Wiley & Sons, **2013**, p. 215.

[36] O. Schiemann, C. A. Heubach, D. Abdullin, K. Ackermann, M. Azarkh, E. G. Bagryanskaya, M. Drescher, B. Endeward, J. H. Freed, L. Galazzo, D. Goldfarb, T. Hett, L. Esteban Hofer, L. Fábregas Ibáñez, E. J. Hustedt, S. Kucher, I. Kuprov, J. E. Lovett, A. Meyer, S. Ruthstein, S. Saxena, S. Stoll, C. R. Timmel, M. Di Valentin, H. S. Mchaourab, T. F. Prisner, B. E. Bode, E. Bordignon, M. Bennati, G. Jeschke, *Journal of the American Chemical Society* **2021**, *143*, 17875–17890.

[37] S. Takahashi, L.-C. Brunel, D. T. Edwards, J. van Tol, G. Ramian, S. Han, M. S. Sherwin, *Nature* **2012**, *489*, Number: 7416 Publisher: Nature Publishing Group, 409–413.

[38] EasySpin Tools, https://easyspin.org/documentation/tools.html.

[39] C. B. Wilson, Physics, University of California, Santa Barbara, Santa Barbara, CA, **2019**.

[40] J. P. Zayner, T. R. Sosnick, *PLOS ONE* **2014**, *9*, Publisher: Public Library of Science, e87074.

[41] A. A. Gil, S. P. Laptenok, J. B. French, J. N. Iuliano, A. Lukacs, C. R. Hall, I. V. Sazanovich, G. M. Greetham, A. Bacher, B. Illarionov, M. Fischer, P. J. Tonge, S. R. Meech, *The Journal of Physical Chemistry B* **2017**, *121*, PMID: 28068090, 1010–1019.

[42] A. I. Nash, W.-H. Ko, S. M. Harper, K. H. Gardner, *Biochemistry* **2008**, *47*, PMID: 19063612, 13842–13849.

[43] D. Nozaki, T. Iwata, T. Ishikawa, T. Todo, S. Tokutomi, H. Kandori, *Biochemistry* **2004**, *43*, PMID: 15222749, 8373–8379.

[44] M. T. Alexandre, R. van Grondelle, K. J. Hellingwerf, J. T. Kennis, *Biophysical Journal* **2009**, *97*, 238–247.

[45] S. Crosson, K. Moffat, *Proceedings of the National Academy of Sciences* **2001**, *98*, Publisher: Proceedings of the National Academy of Sciences, 2995–3000.

[46] K. Ilker Sen, J. Chamoun, P. Fajer, CWdipFit - Dipolar CW analysis program.

[47] EasySpin - EPR spectrum simulation, https://easyspin.org/.

[48] B. D. Zoltowski, B. Vaccaro, B. R. Crane, *Nature Chemical Biology* **2009**, *5*, 827–834.

[49] A. I. Nash, R. McNulty, M. E. Shillito, T. E. Swartz, R. A. Bogomolni, H. Luecke, K. H. Gardner, *Proceedings of the National Academy of Sciences* **2011**, *108*, Publisher: Proceedings of the National Academy of Sciences, 9449–9454.

[50] S. Raffelberg, M. Mansurova, W. Gärtner, A. Losi, *Journal of the American Chemical Society* **2011**, *133*, Publisher: American Chemical Society, 5346–5356.

[51] M. T. A. Alexandre, J. C. Arents, R. van Grondelle, K. J. Hellingwerf, J. T. M. Kennis, *Biochemistry* **2007**, *46*, Publisher: American Chemical Society, 3129–3137.

[52] R. H. Chan, R. A. Bogomolni, *The Journal of Physical Chemistry B* **2012**, *116*, Publisher: American Chemical Society, 10609–10616.

[53] S.-H. Song, P. L. Freddolino, A. I. Nash, E. C. Carroll, K. Schulten, K. H. Gardner, D. S. Larsen, *Biochemistry* **2011**, *50*, Publisher: American Chemical Society, 2411–2423.

[54] P. L. Freddolino, K. H. Gardner, K. Schulten, *Photochemical & Photobiological Sciences* **2013**, *12*, Publisher: The Royal Society of Chemistry, 1158–1170.

[55] D. Singh, Y. Wang, J. Mallon, O. Yang, J. Fei, A. Poddar, D. Ceylan, S. Bailey, T. Ha, *Nature Structural & Molecular Biology* **2018**, *25*, Number: 4 Publisher: Nature Publishing Group, 347–354.

[56] R. Roy, S. Hohng, T. Ha, *Nature Methods* **2008**, *5*, Number: 6 Publisher: Nature Publishing Group, 507–516.

[57] E. D. Holmstrom, A. Holla, W. Zheng, D. Nettels, R. B. Best, B. Schuler in *Methods in Enzymology*, (Ed.: E. Rhoades), Intrinsically Disordered Proteins, Academic Press, **2018**, pp. 287–325.

[58] D. W. Piston, G.-J. Kremers, *Trends in Biochemical Sciences* **2007**, *32*, 407–414.

[59] J. D. Garrett, garrettj403/SciencePlots, version 1.0.9, http://doi.org/10.5281/zenodo.4106649, **2021**.